

FRONT MATTER

Title

- Return of the Ritonavir: A Study on the Stability of Pharmaceuticals Processed in Orbit and Returned to Earth

Authors

Haley C. Bauser¹, Pamela A. Smith², Stephan. D. Parent², Larry R. Chan¹, Ami S. Bhavsar¹, Kenneth H. Condon¹, Andrew McCalip¹, Jordan M. Croom¹, Dale K. Purcell², Susan J. Bogdanowich-Knipp², Daniel T. Smith², Brett A. Cowans², Ruba Alajlouni², Stephen R. Byrn², and Adrian Radocea*¹

Affiliations

- Varda Space Industries, El Segundo, California 90245, United States
- Improved Pharma LLC, West Lafayette, Indiana 47906, United States

*Corresponding author. Email: adrian@varda.com

Abstract

Despite notable progress in realizing the benefits of microgravity, the physical stability of therapeutics processed in space has not been sufficiently investigated. Environmental factors including vibration, acceleration, radiation, and temperature, if not addressed could impact the feasibility of in-space drug processing. The presented work demonstrates the successful recovery of the metastable Form III of ritonavir generated in orbit. The test samples and passive controls containing each of the anhydrous forms of ritonavir; Form I, Form II, Form III, and amorphous exhibit excellent stability. By providing a detailed experimental dataset centered on survivability, we pave the way for the future of in-space processing of medicines that enable the development of novel drug products on Earth and benefit long-duration human exploration initiatives.

Teaser

The metastable Form III of ritonavir was successfully crystallized in orbit and subsequently recovered after reentry to Earth.

MAIN TEXT

Introduction

Early proof-of-concept demonstrations conducted on parabolic flights and on extended microgravity platforms such as the international space station (ISS) have demonstrated the potential benefits of in-space microgravity crystallization for better understanding polymorphism and for supporting pathfinding routes towards novel formulations (1-4). Polymorphic control of active pharmaceutical ingredients is a key concern for safety, manufacturability, and dosing (5,6). Unexpected interconversion from one form to a previously undiscovered, more stable form is often an unwanted scenario, most famously exhibited in the recall of ritonavir (6). As a result, understanding stability

50 and form conversion risks in space environments is a key concern for future space-based
51 medicines and microgravity development (7).

52 Stability testing of pharmaceuticals stored on the International Space Station has
53 highlighted that over a period of two years, a shift in potency was observed – though well
54 within the expected shelf-life of the pharmaceuticals (7,8). Prior studies were limited in
55 scope and focused primarily on chemical degradation during extended storage in orbit.
56 The work raised additional questions to be addressed with solid state characterization of
57 drug materials through standard means employed for pharmaceuticals, namely DSC,
58 Raman and XRPD to understand the solid form evolution. Furthermore, questions on the
59 influence of launch and reentry on the state of drug materials were not sufficiently
60 addressed. Previous studies have been hampered, at least partially, by the limited and
61 infrequent retrieval of materials from orbit and so extensive post-flight characterization to
62 assess both the polymorphic state and chemical stability of pharmaceuticals processed has
63 not yet been shown (9-11). The presented work is the first of its kind to analyze the
64 stability of a pure pharmaceutical ingredient (API) processed in space as prior stability
65 studies focus on marketed pharmaceuticals with their respective excipients and shelf
66 stability mechanisms fully incorporated. By analyzing the stability of the pure API, we can
67 examine the feasibility of in-orbit pharmaceutical development.

68 The HIV protease inhibitor ritonavir was selected for its particularly challenging
69 polymorphic landscape which enables assessment of form interconversion for small
70 molecules crystallized in space (6,12,13). An additional factor for its selection is its
71 suitability for melt/cool crystallization (12,13). The crystallization process was tuned for
72 the production of the metastable Form III from the melt of stable Form II. Form III is the
73 crystalline form most vulnerable to form conversion as compared to the other known
74 anhydrous polymorphs of ritonavir. Process development details were previously
75 published (12). Isolation of metastable forms is a routine aspect of polymorph screening,
76 and though most often stable polymorphs are preferred for final drug products, metastable
77 forms can be selected to improve dosing profiles or serve as enabling intermediates in
78 manufacturing (14,15).

80 Results

82 Overview of Experiment

84 Figure 1 shows an exploded rendering and photo of the crystallization hardware
85 contained within the spacecraft. The hardware features three stainless steel sample vials
86 sealed with a stainless-steel screw-on cap. A PTFE sphere is seated between the cap and
87 the ritonavir Form II powder to enable sealing of the powder under compression. The
88 hardware is controlled with a printed circuit board (PCB) that enables the application of
89 pre-programmed thermal profiles, established from ground-based studies on ritonavir's
90 metastable Form III (12). Temperature control is achieved through the use of film heaters
91 and a Peltier device in thermal contact with the flight vials via an aluminum heat spreader.

92 Sample loading took place on October 21st, 2022. Flight vials were loaded with
93 ~150 mg of ritonavir Form II. In addition to the three vials that underwent crystallization,
94 four ritonavir control samples were placed in the capsule, thermally isolated from the
95 crystallization hardware to ensure that no thermal profile would be applied to the controls.
96 The purpose of these vials was to determine if any environmental factors experienced
97 throughout the capsule's lifetime influence the final form of ritonavir. Examples of factors
98 that could induce form conversion are vibration and shock events on ascent, radiation

99 from the orbital environment, shock events during reentry, and unwanted temperature
100 increases throughout the process of re-entering the atmosphere and returning to Earth
101 (16,17). Control Vial 1 contains amorphous ritonavir, Control Vial 2 contains Form I
102 ritonavir, Control Vial 3 contains Form II ritonavir, and Control Vial 4 contains Form III
103 ritonavir. The order of ritonavir's form stability is amorphous < Form III < Form I < Form
104 II (12,13).

105 In-orbit crystallization is performed inside a compact, unmanned capsule with
106 Earth reentry capabilities. The reentry capsule and on-board crystallization hardware were
107 developed by Varda Space Industries. Power, communication, and propulsion are
108 provided by a Pioneer satellite bus (Rocket Lab, Inc.). The spacecraft was brought to orbit
109 on a SpaceX Falcon 9 rocket on Transporter 8 launched June 12th, 2023. In-orbit
110 crystallization experiments initiated on June 29th, 2023. The melt temperature was held for
111 36 minutes at 131 °C +/- 2 °C. The quench from the melt temperature to the growth
112 temperature occurred at a rate of -50.9 °C/min where it reached a temperature of 77.3 °C
113 before stabilizing. The growth phase temperature was set at 80 °C +/- 4.2 °C for 23.97
114 hours before cooling to 15 °C at a rate of -3.8 °C/min. A duplicate hardware set was
115 operated back on Earth and used to confirm successful crystallization of Form III in a
116 thermal vacuum chamber at a pressure of 0.001 Torr. Figure 2 shows the thermal profile
117 of the terrestrial test compared to the thermal profile applied in microgravity.

118 After in-space crystallization, the capsule remained in orbit for approximately 8
119 months before safely landing at the Utah Test and Training Range on February 21st, 2024.
120 During reentry the test vial temperature did not exceed 23 °C as shown in Figure 3.

121 **Ritonavir Analysis**

122 Upon removal from the capsule in Utah, the crystallized and control samples were
123 sent in a temperature-controlled environment to the Improved Pharma facility in West
124 Lafayette, IN to analyze the material in each vial. Figure 4 shows the X-ray powder
125 diffraction (XRPD) data and Raman spectra of each of the flight vials compared to a
126 reference of Form III. The analysis of all samples crystallized in microgravity indicates all
127 samples consistent are crystalline Form III. Some amorphous background is detectable in
128 the diffraction pattern of the flight vials. We determined that this amorphous background
129 is likely introduced in the process of sample retrieval from the vials and sample
130 preparation for XRPD as opposed to being introduced via factors from orbit or reentry.
131 We were able to do so by isolating crystalline material above the PTFE ball which was
132 removable while remaining intact. XRPD data of this confirmation is shown in the SI.
133 Furthermore, evidence of amorphous material is not detected in the differential scanning
134 calorimetry (DSC) thermogram indicating that the samples are predominantly crystalline
135 Form III.
136

137 Figure 5 shows the XRPD diffractograms, Raman spectra, and DSC thermograms
138 of the control vials that did not undergo crystallization in microgravity. All control
139 samples, regardless of relative physical stability, were found to be of the same crystal
140 form as packed without detectable amorphous background. This indicates that neither in-
141 orbit radiation nor conditions upon reentry cause polymorph conversion of ritonavir or
142 crystallization of the amorphous ritonavir. Table 1 summarizes the result of all vials in the
143 W-1 capsule.
144
145
146

147 Discussion

148 Our presented results demonstrate the feasibility of processing pharmaceuticals in
149 microgravity. Autonomous operation and reentry expand access to in-orbit processing of
150 pharmaceuticals. The presented work demonstrates excellent thermal control both in-orbit
151 and throughout recovery. For the thermal profile investigated, the polymorphic outcome
152 for ritonavir crystallized from its melt is unchanged when compared to results on Earth.
153 This result is due to the underlying crystallization mechanisms as well as the selection of a
154 process that strongly favors formation of Form III (12,18,19). Future work will examine
155 polymorphic outcomes in microgravity by not only examining additional molecules, but
156 also by expanding the range of thermal profiles examined, including probing behavior at
157 the interface between known or anticipated polymorphic outcomes. The results highlight
158 the importance of careful considerations of crystallization kinetics, thermophysical
159 properties of crystals and their melts, including density, viscosity, and diffusion
160 coefficients alongside ground-based studies to help inform process sensitivity to
161 gravitational forces (20-22). By demonstrating stability, this work enables a path towards
162 in-space processing of pharmaceuticals that not only enables the development of novel
163 drug products for use on Earth, but also contributes to the feasibility of long-duration
164 human exploration initiatives.

165 Materials and Methods

166 Preparation of Ritonavir

167
168 Form II ritonavir was sourced from USP lot M-RIT/0804007. In the preparation of
169 Form I, 206.3 mg of Form II Ritonavir was dissolved in approximately 6 mL or more of
170 ethyl acetate (EtOAc) with the application of heat, approximately 70 °C. The solution was
171 then allowed to cool to room temperature and left to stand overnight without any
172 observable change. Subsequently, a rapid evaporation process was employed to reduce the
173 volume by approximately half. To this concentrated solution, cold hexane (approximately
174 14 mL) was added slowly with continuous stirring, resulting in the immediate formation
175 of a white precipitate which then transitioned into a sticky mass. The mixture was then
176 vigorously vortexed, slightly warmed, and stirring was maintained at room temperature.
177 Afterward, the mixture was placed in the freezer overnight. The resulting precipitant was
178 recovered with filtration through a Swinnex filter assembly equipped with a nylon
179 membrane of 25 mm diameter and 0.2 µm pore size.
180
181

182
183 In the preparation of Form III, 651.4 mg of Form II Ritonavir was evenly spread
184 on a glass microscope slide and compressed to an approximate thickness of 1 mm. The
185 slide was then placed in an oven set at roughly 130 °C, where the solid melted completely
186 within about 25 minutes. After melting, the slide was transferred to an oven maintained at
187 80 °C and left there for approximately 24 hours. Upon removal, the sample was cooled to
188 room temperature, and the presence of some crystals within the glass matrix was
189 confirmed under a microscope. The sample was then returned to the 80 °C oven overnight,
190 but no further changes were observed microscopically. Subsequently, the sample was
191 placed back in the 130 °C oven, where it melted in roughly one minute. The oven
192 temperature was then gradually reduced to approximately 83 °C, and the sample was left
193 overnight. The following day, the white to light tan solids were removed from the oven
194 and cooled to room temperature. The sample appeared fully crystalline under microscopic
195 examination. The final step involved removing the crystalline material from the slide and
196 gently crushing it into a fine powder.

197
198 In the preparation of the amorphous Ritonavir, 904.8 mg of Form II Ritonavir was
199 placed on a glass microscope slide and compressed to approximately 1 mm thickness. The
200 slide was then placed in an oven preheated to approximately 130 °C, where the solid
201 melted completely within approximately 10 minutes. Following this, the molten sample
202 was rapidly quenched on a cold aluminum block taken from the freezer. The sample was
203 then carefully removed from the slide.
204

205 Each sample, weighing 150 ± 1 mg, was carefully transferred into vials within a
206 glove bag purged with inert, dry nitrogen gas to ensure an oxygen- and moisture-free
207 environment.
208

209 XRPD

210
211 XRPD patterns were collected on a PANalytical Empyrean diffractometer using a
212 Cu K α incident beam of radiation generated at 45 kV / 40 mA. A silicon standard was
213 analyzed to verify the observed position of the Si <111> peak is consistent with the NIST-
214 certified position. Powder samples were sandwiched between 3- μ m-thick Etnom films and
215 analyzed in transmission geometry. The X-ray source was configured with Soller slits of
216 0.02 radians, a fixed anti-scatter slit of $1/2^\circ$, a mask of 20 mm, and a fixed divergence slit
217 of $1/2^\circ$. The diffracted beam passed through a 3.0 mm anti-scatter extension and Large
218 Soller slits of 0.02 radians to the detector. A beam-stop was used to minimize the
219 background generated by air. Diffraction patterns were collected with Data Collector
220 software using a PIXcel3D-Medipix3 detector located 240 mm from the specimen. The
221 data was acquired using a single scan from $2-50^\circ 2\theta$ with the sample spinning at a
222 revolution time of 2 seconds.
223

224 Raman Spectroscopy

225
226 A HORIBA Scientific XploRA Series Confocal Raman Microscope (Piscataway,
227 NJ) was used to collect Raman spectra using the following parameters: 785 nm laser at
228 100% power, 1200 g/mm grating, 300 micrometer confocal hole, 100 micrometer slit
229 entrance to the spectrograph, 1 second spectra acquisition with 30 accumulations. The
230 Raman signal is detected using a Sincerity Model 356399, thermoelectrically cooled CCD
231 detector. Spectra were acquired over the range -125 to 1800 cm^{-1} . An Olympus Series
232 BX51TRF polarized light microscope (Olympus America Inc., Melville, NY) provided the
233 base optical platform. An Olympus MPlan N Series 20X, 0.40 NA microscope objective
234 was used to focus the laser light onto the sample and to collect the Raman signal. The
235 microscope was equipped with a Marzhauser Wetzlar computer-controlled mapping stage
236 to translate the sample for focus and data acquisition. Digital images were acquired using
237 a Lumenera Series Infinity 3-1C (Teledyne Lumenera, Ottawa, Ontario, Canada) camera
238 using Infinity software version 6.5.6 and Infinity Analyze software version 7.0.2.930
239 (Build data 1-May-2020). System calibration was performed prior to analysis using a
240 silicon disc to monitor peak position at 520.7 cm^{-1} .
241

242 The sample was prepared for analysis by placing a small amount of material onto a
243 gold-coated microscope slide using a tungsten needle and dispersed to a thin layer. The
244 small sample was illuminated with white light using 200X magnification for specific
245 sample area analysis.
246

DSC

DSC was performed using a TA Instruments model Q10 differential scanning calorimeter. The instrument was calibrated using indium. The sample was placed into a standard aluminum DSC pan, covered with a lid that was manually pierced with a pin, and the weight was accurately recorded. The pan lid was crimped prior to sample analysis. An aluminum pan configured as the sample pan was placed on the reference side of the cell. The sample was analyzed in a single run from 20 to 200 °C at a heating rate of 10 °C/min under a purge of nitrogen (50 cc/min).

References

1. Y. Zhang, J. Cheng, Y. Glick, G. Samburski, J. Chen, C. Yang, Antisolvent crystallization of L-histidine in micro-channel reactor under microgravity *Microgravity Science and Technology* **32**, 27-33 (2020).
2. S. Amselem Remote controlled autonomous microgravity lab platforms for drug research in space *Pharmaceutical Research* **36**, 183 (2019).
3. M. A. Giulianotti and L. A. Low, Pharmaceutical research enabled through microgravity: Perspectives on the use of the international space station U.S. national laboratory *Pharmaceutical Research* **37**, 1 (2020).
4. P. Reichert, W. Prorise, T. O. Fischmann, G. Scapin, C. Narasimhan, A. Spinale, R. Polniak, X. Yang, E. Walsh, D. Patel, W. Benjamin, J. Welch, D. Simmons, C. Strickland, Pembrolizumab microgravity crystallization experimentation *npj Microgravity* **5**, A28 (2019).
5. S. R. Byrn, R. R. Pfeiffer, J. G. Stowell *Solid-state chemistry of drugs* (SSCI, Inc., 1999).
6. J. Bauer, S. Spanton, R. Henry, J. Quick, W. Dziki, W. Porter, J. Morris, Ritonavir: an extraordinary example of conformational polymorphism *Pharmaceutical Research* **18**, 859-866 (2001).
7. P. M. Williams, T. Shivakumar, V. Anyanwu, "Space Medicine and Countermeasures" in *In-Space Manufacturing and Resources* (Wiley Online Books, 2022).
8. J. F. Reichard, S. E. Phelps, K. R. Lenhardt, M. Young, B. D. Easter, The effect of long-term spaceflight on drug potency and the risk of medication failure *npj Microgravity* **9**, A35 (2023).
9. M. Gresko, Panel calls for giant boost to space station research *Science* **381**, 1144-1145 (2023).
10. J. Foust, NASA hits limits of space station utilization *Space News* (January 31, 2023).
11. J. Foust, SpaceX revamps smallsat rideshare program *Space News* (August 29, 2019).
12. S. D. Parent, P. A. Smith, D. K. Purcell, D. T. Smith, S. J. Bogdanowich-Knipp, A. S. Bhavsar, L. R. Chan, J. M. Croom, H. C. Bauser, A. McCalip, S. R. Byrn, A. Radocea, Ritonavir form III: A coincidental concurrent discovery *Crystal Growth & Design* **23**, 320-325 (2022).
13. X. Yao, R. F. Henry, G. G. Z. Zhang, Ritonavir Form III: A new polymorph after 24 years *Journal of Pharmaceutical Sciences* **112**, 237-242 (2022).

- 290 14. R. Censi and P. D Martino, Polymorph impact on the bioavailability and stability of
291 poorly soluble drugs *Molecules* **10**, 18759-18776 (2015).
- 292 15. A. Y. Sheikh, A. Mattei, R. M. Bhardwaj, R. S. Hong, N. A. Abraham, G. Schneider-
293 Rauber, K. M. Engstrom, M. Diwan, R. F. Henry, Y. Gao, V. Juarez, E. Jordan, D. A.
294 DeGoey, C. H. Hutchins, Implications of the conformationally flexible, macrocyclic
295 structure of the first-generation, direct-acting anti-viral paritaprevir on its solid form
296 complexity and chameleonic behavior *Journal of the American Chemical Society* **143**,
297 17479-17491 (2021).
- 298 16. “Rideshare Payload User’s Guide (SpaceX, 2021).
- 299 17. R. G. Finke, Calculation of reentry-vehicle temperature history *Institute for Defense*
300 *Analysis* IDA Paper P-2395 (1990).
- 301 18. M Mohr and H. Fecht, Investigating thermophysical properties under microgravity: A
302 review *Advanced Engineering Materials* **23**, 2001223 (2021).
- 303 19. J. A. Baird, B. Van Eerdenbrugh, L. S. Taylor, A classification system to assess the
304 crystallization tendency of organic molecules from undercooled melts *Journal of*
305 *Pharmaceutical Science* **99**, 3787-3806 (2010).
- 306 20. P. W. G. Poodt, P. C. M. Christianen, W. J. P. van Enkevort, J. C. Maan, E. Vlieg. The
307 critical Rayleigh number in low gravity crystal growth from solution *Crystal Growth and*
308 *Design* , 2194-2199 (2008).
- 309 21. E. H. Snell and J. R. Helliwell, Macromolecular crystallization in microgravity *Reports on*
310 *Progress in Physics* **68**, 799 (2005)
- 311 22. K. Pal and A. Radocea, Gravity as a knob for tuning particle size distributions of small
312 molecules *Crystal Growth and Design* (2024).
- 313
314

315 Acknowledgments

316
317 The authors acknowledge the mission operations team at Varda Space Industries and
318 Rocket Lab, Inc. for their work in maintaining the capsule throughout its life cycle. The
319 authors acknowledge Brandon Amat, Tracy Vu, and Kris Stone for their recovery of the
320 capsule and safe retrieval of the experimental vials. The authors acknowledge Aakash
321 Patel for integration and testing support. The authors acknowledge Sarah Parent for her
322 photography of the hardware.

323

324 Author contributions:

325 Conceptualization: AR, JMC, SRB, HCB
326 Hardware Development: LRC, ASB, KHC, AM, JMC
327 Process Development: HCB, SRP, PAS, BAC, ASB, JMC, AR
328 Analysis: PAS, SRP, HCB, RAA, DKP, SJB, DTS
329 Writing—original draft: HCB
330 Writing—review & editing: HCB, AR, PAS.

331

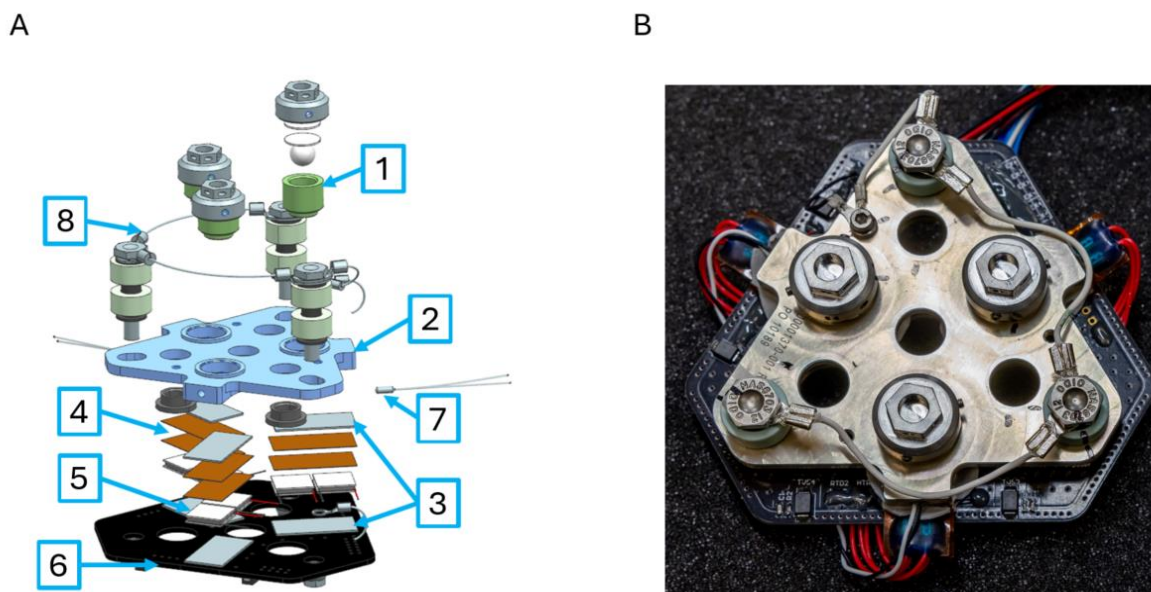
332 **Competing interests:** The authors declare the following competing financial interest(s):
333 Varda Space Industries participated in the experimental design, research, data
334 interpretation and analysis, writing, reviewing, and approval of the publication. H.C.
335 Bauser, A.S. Bhavsar, A. McCalip, L.R. Chan, K. H Condon, J.M. Croom, and A.

336 Radocea are employees of Varda Space Industries and may own Varda Space Industries
337 stock.

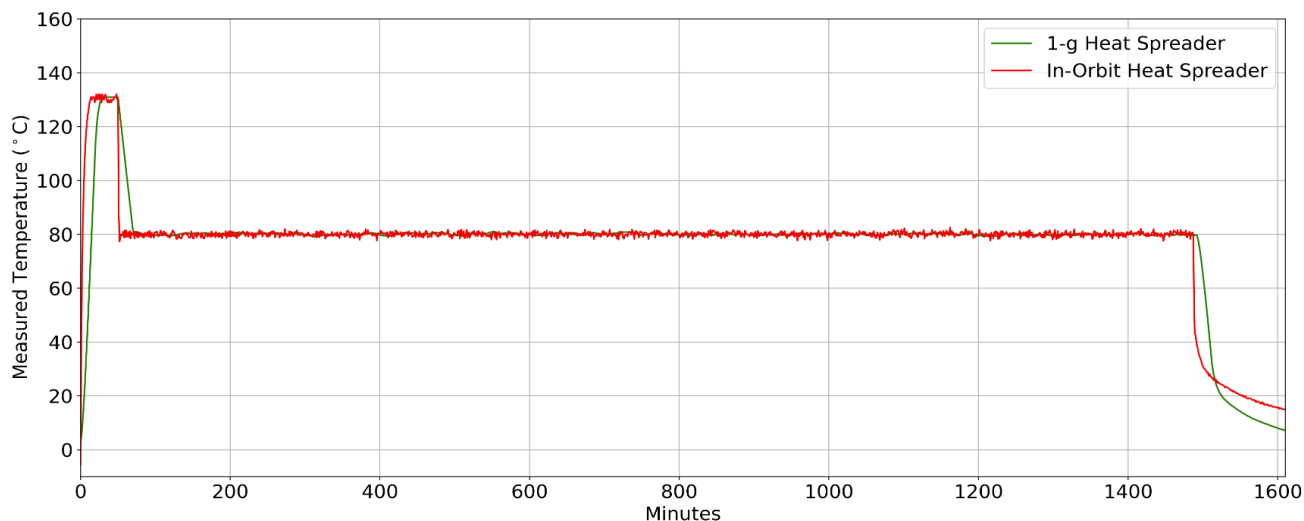
338
339 **Data and materials availability:**

340 All data are available in the main text or the supplementary materials.

341
342 **Figures and Tables**

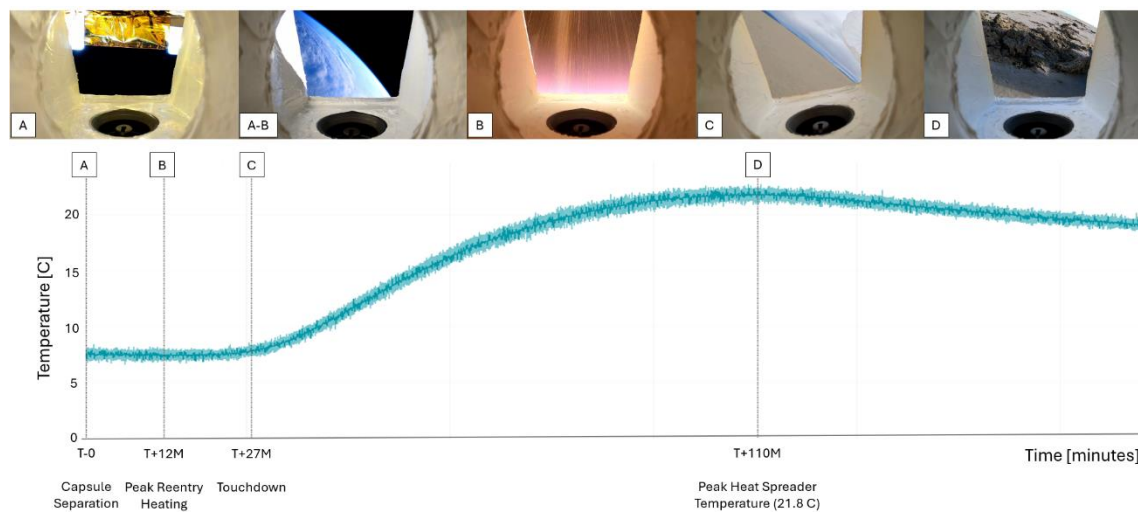


343
344 **Fig. 1. Overview of the in-orbit crystallization hardware. (A)** Exploded view of the
345 Varda PCB Stack and API vials. The components are as follows. 1) (3x) 316 Stainless
346 Steel vials each holding ~150 mg of API, sealed with a PTFE ball and spacers. 2) 6061
347 Aluminum plate heat spreader holding the vials and the resistance temperature detectors
348 (RTDs). 3) Thermal interface material 4) (6x) Kapton film heaters each with a total power
349 of 23 watts 5) (6x) Peltier devices used in both forward bias for cooling and reverse bias
350 for additional heater power 6) PCB 7) (2x) RTDs in heat spreader and 1x RTD on the
351 ballast side of the PCB 8) grounding wires. **(B)** Picture of the fully assembled Varda PCB
352 Stack.



354
355
356

Fig 2. Temperature Profile in 1-g and In-Orbit. Comparison of the heat spreader temperature during the 1-g crystallization of ritonavir and the heat spreader temperature during the in-orbit crystallization of ritonavir.



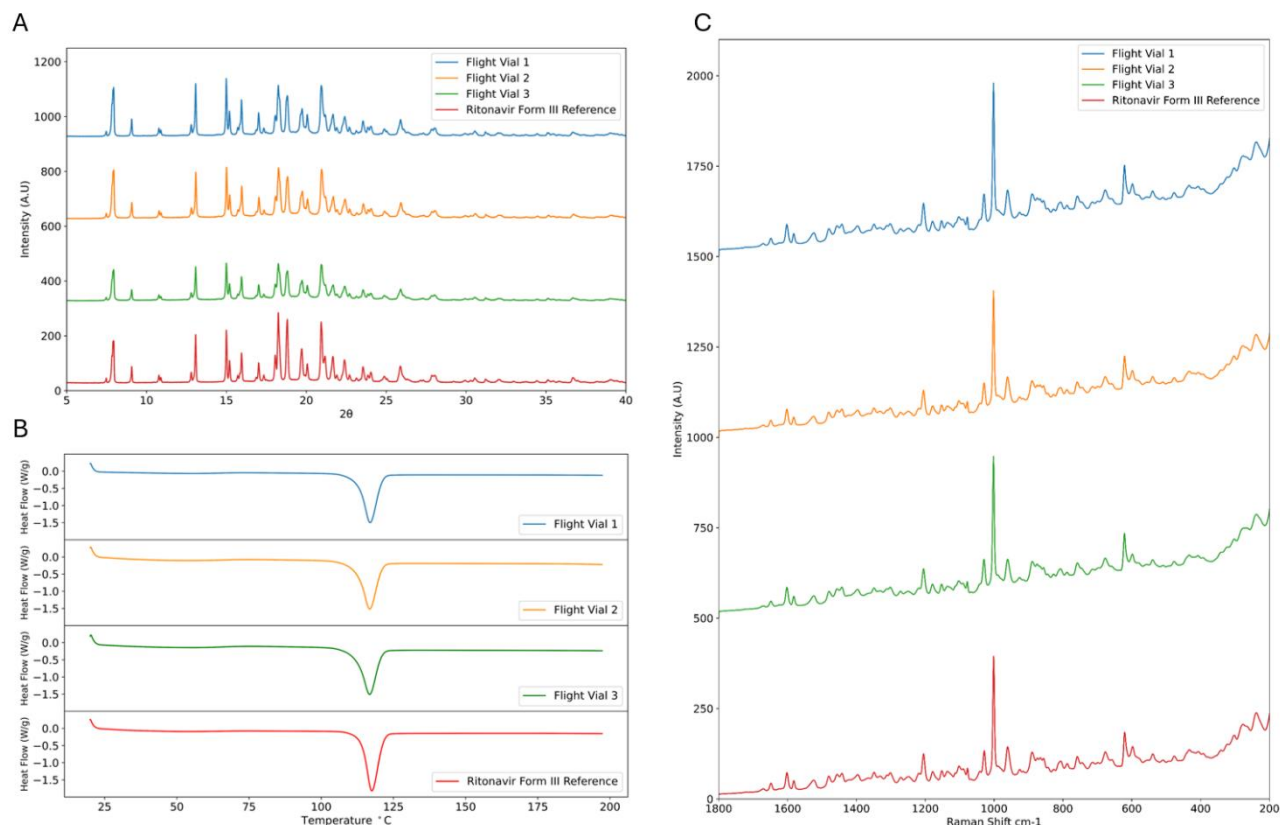
357

358
359
360
361
362
363

Fig 3. Timeline of Heat Spreader Temperature Throughout Reentry with Corresponding Images from Capsule. (A) Image and corresponding heat spreader temperature upon capsule separation from the Pioneer satellite. (A-B) Image shows the capsule above Earth independent of the satellite. (B) Image and corresponding heat spreader temperature at the maximum capsule external temperature during reentry. (C) Image and corresponding heat spreader temperature upon capsule touchdown in Utah. (D)

364
365
366

Image and corresponding heat spreader temperature at maximum temperature experienced while awaiting recovery.



367
368
369
370
371
372
373
374
375
376
377
378
379
380
381
382
383
384
385

Fig 4. Analysis of Samples Crystallized in Microgravity. (A) Diffractograms of material extracted from each of the three vials that underwent crystallization in-orbit. All three vials match the Form III reference material. (B) Thermograms of material extracted from each of the three vials that underwent crystallization in-orbit. All three vials match the endotherm of Form III. The melt temperatures are 116.94 °C, 116.77 °C, 116.73 °C, respectively and the heat capacities are 50.54 J/g, 51.78 J/g, and 51.11 J/g, respectively (C) Raman spectra of material extracted from each of the three vials that underwent crystallization in orbit. The presented spectra are averages of the spectra of 10 samples from each of the vials to ensure adequate representation across the crystalline material.

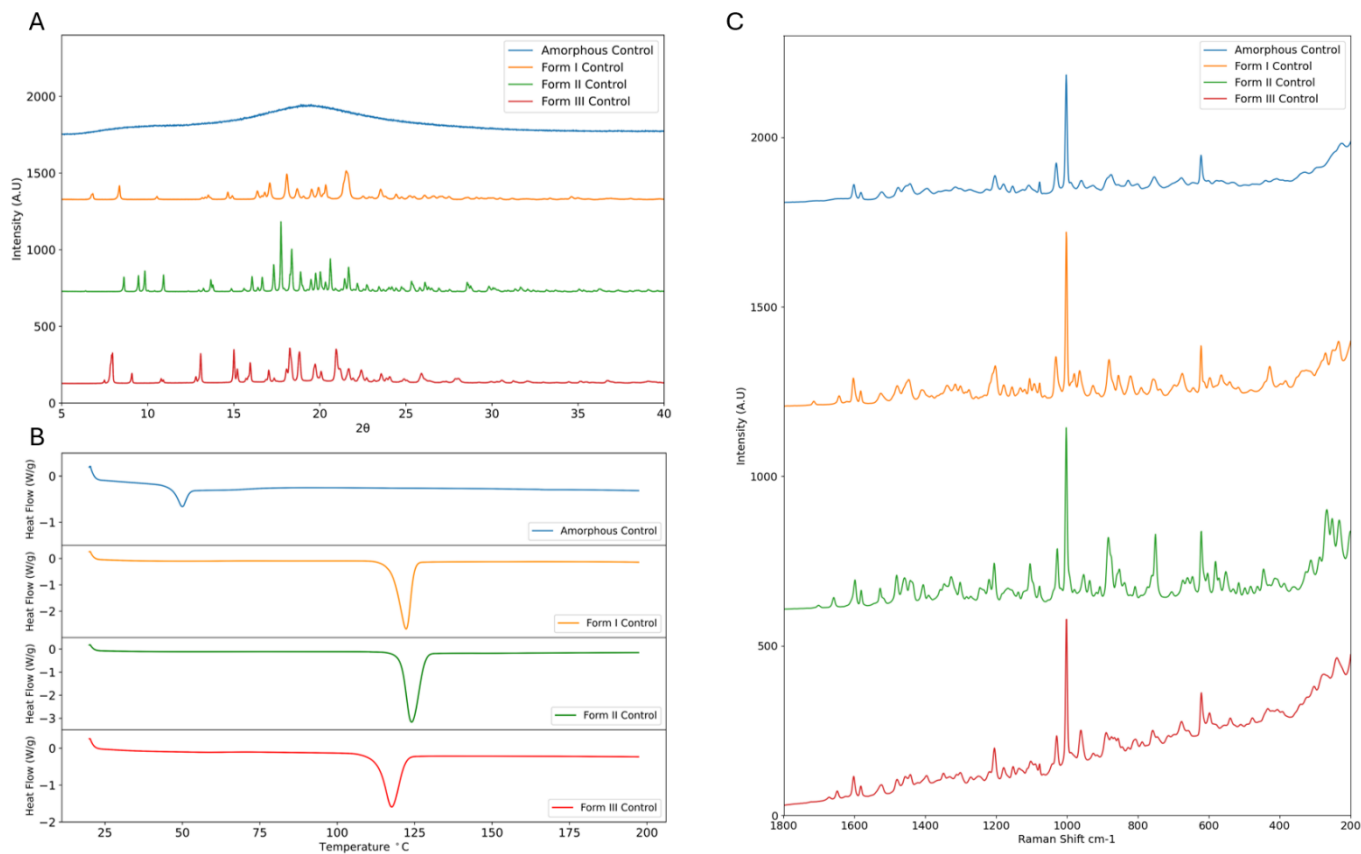


Fig 5. Analysis of In-Orbit Control Samples. (A) Diffractograms of material extracted from the control vials. All diffraction patterns match that of their initially packed form (B) Thermograms of material extracted from each of the control vials. All endotherms match that of their form as packed. The melting temperatures are 50.0 °C, 122.25 °C, 124.00 °C, and 117.52 °C, respectively. The heat capacity of Form I is 76.46 J/g, the heat capacity of Form II is 94.23 J/g, and the heat capacity of Form III is 53.13 J/g. (C) Raman spectra of material extracted from the control vials. All spectra match that of their initially packed form. The presented spectra are each an average of the spectra of 10 samples from each of the vials to ensure adequate representation across the crystalline material.

411 **Table 1. Summary of Flight Sample Crystallinity**

Sample ID	Starting Material	In-Orbit Crystallization	Post Reentry Material
Flight Vial 1	Ritonavir Form II	Yes	Ritonavir Form III
Flight Vial 2	Ritonavir Form II	Yes	Ritonavir Form III
Flight Vial 3	Ritonavir Form II	Yes	Ritonavir Form III
Control Vial 1	Amorphous Ritonavir	No	Amorphous Ritonavir
Control Vial 2	Ritonavir Form I	No	Ritonavir Form I
Control Vial 3	Ritonavir Form II	No	Ritonavir Form II
Control Vial 4	Ritonavir Form III	No	Ritonavir Form III

412

Supplementary Materials for

Return of the Ritonavir: A Study on the Stability of Pharmaceuticals Processed in Orbit and Returned to Earth

Haley C. Bauser¹, Pamela A. Smith², Stephan. D. Parent², Larry R. Chan¹, Ami S. Bhavsar¹, Kenneth H. Condon¹, Andrew McCalip¹, Jordan M. Croom¹, Dale K. Purcell², Susan J. Bogdanowich-Knipp², Daniel T. Smith², Brett A. Cowans², Ruba Alajlouni², Stephen R. Byrn², and Adrian Radocea*¹

1. Varda Space Industries, El Segundo, California 90245, United States
2. Improved Pharma LLC, West Lafayette, Indiana 47906, United States

*Corresponding author. Email: adrian@varda.com

This PDF file includes:

Figs. S1 to S2
Table S1

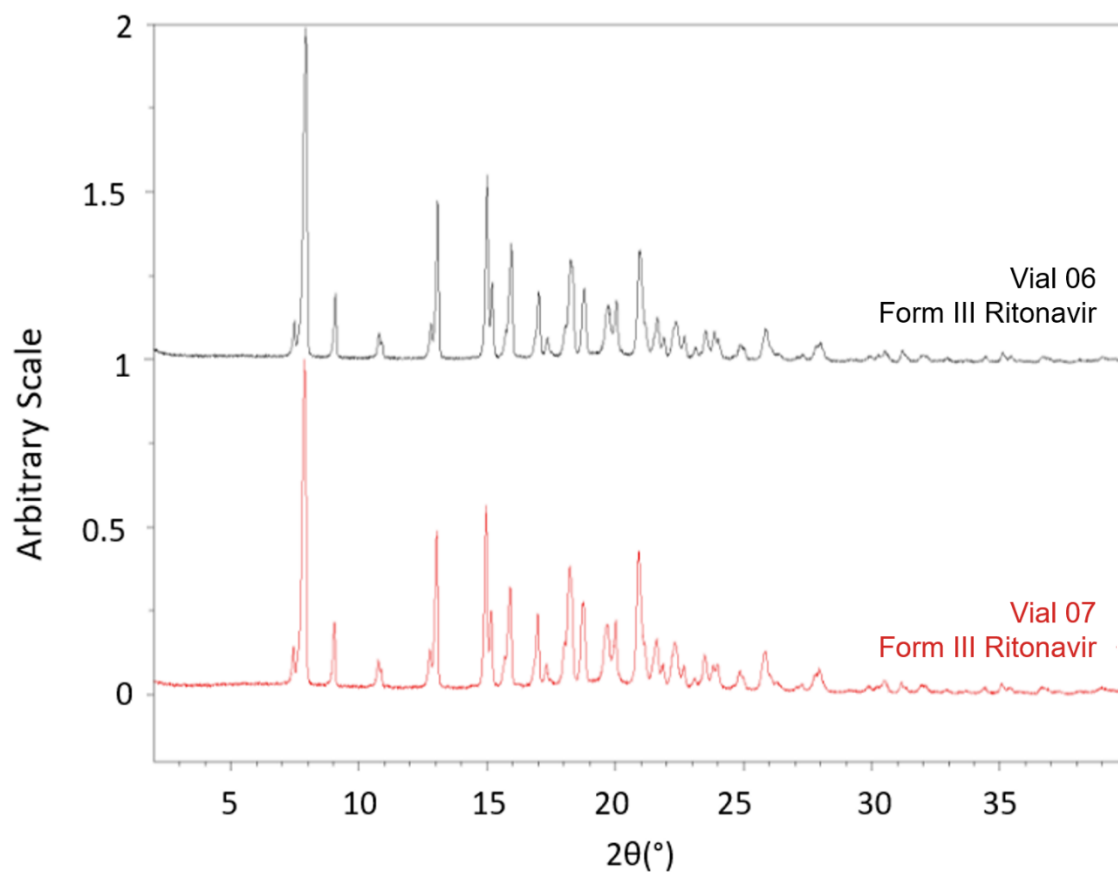


Fig S1. Resulting Crystallinity from Terrestrial Crystallization Test. XRPD diffractograms of ritonavir crystallized in the crystallization hardware terrestrially under vacuum. Both sample patterns match that of Form III.

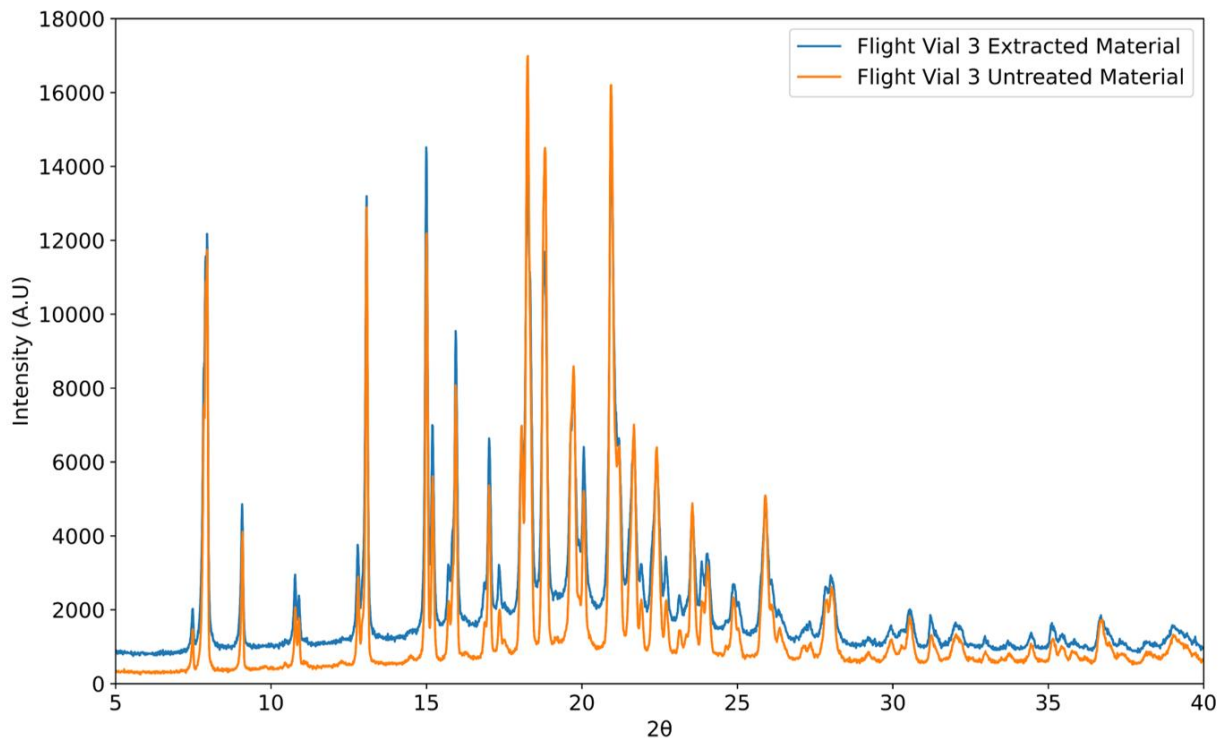


Fig S2. XRPD of untreated material vs. extracted and lightly ground material. The diffraction pattern of the extracted material from Flight Vial 3 contains some amorphous background that can be attributed to the process of removing the materials from the vials and lightly grinding for XRPD measurement. The untreated material was removed in a large piece from the Teflon ball seal and was therefore not subjected to the same removal force as the bulk of the material from Flight Vial 3. The untreated material does not have the same amorphous background indicating the extraction is the likely cause of the amorphous background instead of the forces during reentry.

Table S1. Thermal recipe compared to as-measured terrestrial and in-orbit performance.

		Recipe	Terrestrial	Microgravity
Melt Phase	Melt Ramp Rate	Any	11.2 °C/min	9.6 °C/min
	Melting Temperature	131 °C +/-3 °C	130 °C +/-1 °C	131°C +/-2 °C
	Melt Duration	> 20 min	38.4 min	36 min
	Melt Quench Rate	≤-20 °C/min	-29 °C/min	-50.9 °C/min
	Melt Quench Min Temp	75 °C	77.7 °C	77.3 °C
Growth Phase	Growth Temperature	80 °C +/-3 °C	80 °C +/-0.5 °C	80 °C +/-4.2 °C
	Growth Duration	24 hours +/- 1hour	23.6 hours	23.83 hours
	Growth Quench Rate	Any	-4.5 °C/min	-3.8 °C/min